HEFAT2012
9th International Conference on Heat Transfer, Fluid Mechanics and Thermodynamics
16 – 18 July 2012
Malta

THREE DIMENSIONAL SIMULATION TO OBSERVE THE EFFECTS OF THE STATIC MAGNETIC FIELD ON THE GROWTH OF $Si_{0.25}Ge_{0.75}$ IN A VERTICAL BRIDGMAN SETTING

Shemirani M.M.[1], Chacha M.[1]* and Saghir M.Z.[2]
*Author for correspondence
[1]Department of Mechanical and Industrial Engineering,
ALHOSN University,
P.O. Box 38772, Abu Dhabi,
United Arab Emirates
Tel: +971 2 4070 516 Fax: +971 2 4070 799 E-mail: m.chacha@alhosnu.ae
[2]Department of Mechanical and Industrial Engineering,
Ryerson University,
350 Victoria Street, Toronto, ON, M5B 2K3,
Canada

ABSTRACT

A numerical modeling and simulation of single bulk crystals of $Si_{0.25}Ge_{0.75}$ growth with Si rich is conducted to investigate the effect of static magnetic field on the heat and mass transfer in the solvent region in a vertical Bridgman furnace. The curvature and shape of the silicon concentration in the process of crystallization near the growth interface are also examined. Different magnetic field intensities were applied. The meridianal flow as well as the azimuthal flow in the solvent region under the applied polynomial temperature along the vertical dimension of the model were investigated and it was found that the axial magnetic field does not have effective influence on the buoyancy induced convection in the solvent region.

NOMENCLATURE

B	[T]	Magnetic field induction
C	[-]	Dimensionless concentration
c	[-]	Solute concentration (atomic %)
r	[m]	Radial coordinate
R	[m]	Dimensionless radial coordinate
$\mathbf{V}$	[m/s]	Dimensionless velocity vector
V	[-]	Dimensionless velocity component
z	[m]	Axial coordinate
Z	[-]	Dimensionless axial coordinate

Special characters

α	[m^2/s]	Mass diffusivity
β	[1/at % Si]	Solutal expansion coefficient
φ	[rad]	Circumferential (azimuthal) direction
τ	[-]	Dimensionless time
θ	[-]	Dimensionless temperature
Ω	[rad/s]	Rotational speed
ω^*	[-]	Dimensionless angular velocity
∇	[1/m]	Nabla operator

Subscripts

0	Reference
1, r	r-component
2	φ-component
3, z	z-component
c	Mass, species, solutal
m	Melt
T	Temperature

INTRODUCTION

In response to the global demand for electronic devices such as life saving medical equipment, wireless communication sets, and solar collector cells, a corresponding need for flawless and defect free semiconductors is inevitable IUPAC [1]. Semiconductor defects happen in the process of crystal growth at the solidification stage. The reliability of the aforementioned products is highly dependent on the performance of the semiconductors being used in them. This reliance is based on the consistency of the internal arrangement of atoms in a three dimensional crystal structure and characteristics such as uniformity and purity of bulk single crystals. The authors of this paper have shown in their previous studies how to suppress the buoyancy induced convection which is an undesirable factor in the process of bulk single crystal growth in both terrestrial and microgravity condition by applying magnetic field and employing the travelling solvent method (TSM). In

this paper we are attempting to investigate the effects of static magnetic field of the growth of $Si_{0.25}Ge_{0.75}$ by utilizing the Bridgman technique. Application of magnetic fields in semiconductor crystal growth is an efficient solution to control the convection in the liquid, the micro and macro segregation and to improve the material quality. Nowadays, growth installations can be equipped with different magnetic field configurations. Transverse, axial and cusp static magnetic fields are used to eliminate thermal fluctuations and to damp thermal convection in the liquid in order to obtain stable transport regimes [2]. It has been observed that the intensity of the melt convection has a significant influence on both radial and axial segregation of species and interface shape during crystal growth. Studies of natural convection in the melt have demonstrated that the magnitude of the radial segregation is lower than the axial one and is due to either a) diffusion-controlled growth such as convection free or b) intense mixing in the melt [3, 4]. The radial segregation reaches a maximum for intermediate values of flow intensity, which results in relatively thick solute boundary layers that have a non-uniform thickness [5]. When crystals are grown in the Bridgman configuration, forced convection is difficult to produce, because the crystal cannot be moved relative to the ampoule. The intensity of the natural convection which cannot be avoided scales with the (thermal) Grashof number. It is obvious that the intensity of the buoyancy driven convection depends highly on the melt height and thus changes as the melt is depleted [6]. In the vertical Bridgman configuration for crystal growth, the interface shape is a factor that greatly influences the yield of single crystals. The shape of the interface is mainly determined by the temperature field near the interface and the level of natural convection in the melt [7]. The shape of the interface can range from concave to convex. Slightly convex interface shape is most desirable because it eliminates most problems with spontaneous nucleation at the crucible wall and improves grain selection which results in higher yield of single crystals. However, the efforts of obtaining convex interface shapes in growth experiments have been of limited success [8]. A planar interface shape has the beneficial effect of minimizing thermal stresses and the intention of the present work is to establish a desirable interface shape by controlling the convection in the melt and the directional heat flux near the interface by means of the static magnetic field.

MODEL DESCRIPTION

The model consists of a fixed cylindrical coordinate system (r, φ, z) with its origin located at the center of the solid section (seed). The model is 11.5 cm long with a uniform diameter of 2.5 cm and consists of two segments as; seed (Silicon) 2.5 cm, the solvent region 9cm which is a mixture of silicon (Si) and germanium (Ge) initially set as $Ge_{0.75}Si_{0.25}$, which is the upper segment. The vertical Bridgman method is the technique being chosen for this study. Both sections, introduced earlier in model description, are held in a quartz ampoule. A polynomial temperature profile with minimal temperature difference between top and the bottom of the model is applied on the outer face of the crucible. Since the melt temperature of the solvent region is much less than that of the quartz, there would be no oxygen penetration from quartz into the melt and consequently no contamination or impurity occurs which is a great advantage of low temperature gradient in this technique. Figure 1 depicts the model under study.

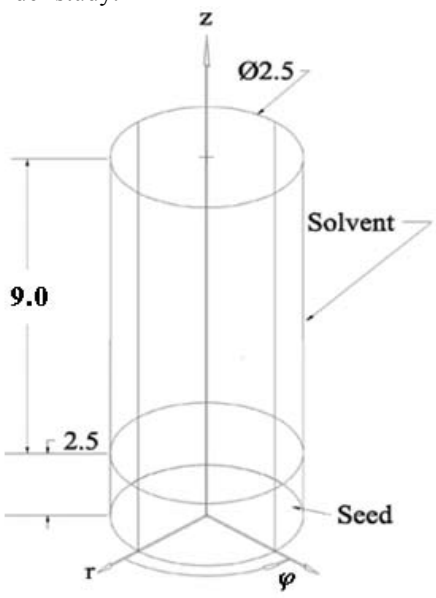

Figure 1 Bridgman model region under investigation

The main physical properties of the solvent are presented in the Table 1.

Table 1. Physical Properties of $Ge_{0.75}Si_{0.25}$

Symbol	Values	Units
c_p	0.4145	J/g/K
T_m	1057.5	ºC
α_c	1.65×10^{-4}	cm^2/s
σ	2.5×10^{4}	S/cm
β_c	0.005	/at% Si
β_T	5.075×10^{-6}	1/ºC
κ	0.294	W/cm/K
μ	4.3×10^{-3}	g/cm/s
ρ	4.843	g/cm^3

GOVERNING EQUATIONS

Navier-Stokes equations: the laminar Newtonian fluid's motion is governed by the Navier-Stokes equations described and solved for each direction of the cylindrical coordinate system in steady state; taking Boussinesq approximation into

account. In the non-dimensional forms the governing equations are as follow:

r-component:

$$Re\left((\mathbf{V}\cdot\nabla)V_r-\frac{V_\varphi^{\,2}}{R}\right)=-\frac{\partial P}{\partial R}+\nabla^2 V_r-\frac{V_r}{R^2}-\frac{2}{R^2}\frac{\partial V_\varphi}{\partial\varphi} \quad (1)$$
$$+Ha^2\left(V_z B_1^* B_3^*-V_r(B_3^{*2}-B_2^{*2})+V_\varphi B_1^* B_2^*\right)+\frac{(Gr_T)_r}{Re}\theta-\frac{(Gr_C)_r}{Re}C$$

φ-component:

$$Re\left((\mathbf{V}\cdot\nabla)V_\varphi+\frac{V_r V_\varphi}{R}\right)=-\frac{1}{R}\frac{\partial P}{\partial\varphi}+\left(\nabla^2 V_\varphi-\frac{V_\varphi}{R^2}+\frac{2}{R^2}\frac{\partial V_r}{\partial\varphi}\right) \quad (2)$$
$$+Ha^2\left(V_r B_1^* B_2^{*2}-V_\varphi(B_1^{*2}-B_3^{*2})+V_z B_2^* B_3^*\right)+\frac{(Gr_T)_\varphi}{Re}\theta-\frac{(Gr_C)_\varphi}{Re}C$$

z-component:

$$Re(\mathbf{V}\cdot\nabla)V_z=-\frac{\partial P}{\partial Z}+\nabla^2 V_z \quad (3)$$
$$+Ha^2\left(V_\varphi B_3^* B_2^*-V_z(B_2^{*2}-B_1^{*2})+V_r B_1^* B_3^*\right)+\frac{(Gr_T)_z}{Re}\theta-\frac{(Gr_C)_z}{Re}C$$

The above equations (1-3) are the momentum equations in the solvent region in the radial (r), angular (φ) and axial (z) directions; with gravity and magnetic body forces. Re is the Reynolds number and Ha, is the Hartman number (non-dimensional form of the magnetic field effect). The magnetic field is assumed to be perfectly aligned with the axis of the model furnace (see Appendix A), therefore the two components B_1 (r-direction) and B_2 (φ -direction) are set equal to zero [9]. In the above equations Gr_T is the thermal Grashof number and Gr_C is the solutal Grashof number.

Energy equation: the energy equation is defined for the solvent region's as follows:

$$(\mathbf{V}\cdot\nabla)\theta=\frac{\nabla^2\theta}{Re.Pr} \quad (4)$$

Where Pr is the Prandtl number.

Continuity equation: the solvent's continuity equation reads as:

$$\frac{1}{R}\frac{\partial}{\partial R}(RV_r)+\frac{1}{R}\frac{\partial V_\varphi}{\partial\phi}+\frac{\partial V_z}{\partial Z}=0 \quad (5)$$

***Solute equation*:** the mass transfer is governed by the following equation:

$$(\mathbf{V}\cdot\nabla)C=\frac{\nabla^2 C}{Re.Sc} \quad (6)$$

Where the solutal diffusion coefficient is represented by the (dimensionless) Schmidt number, Sc.

Boundary conditions: in this model, the boundary conditions are as follow:

a) At the ampoule side wall (solid):

$$V_r=V_\varphi=V_z=0\ ;\ \frac{\partial C}{\partial R}=0 \quad (7)$$

b) At the dissolution interface which is on the top horizontal surface:

$$C=C_1=0.50 \quad (8)$$

c) At the solid interface which is on the bottom horizontal section:

$$C=C_2=0.25 \quad (9)$$

Where c_1 and c_2 represent the silicon concentration in the feed and solvent respectively.

d) At the external surface of the quartz ampoule (not shown in Fig. 1) a polynomial temperature profile is applied in the z-direction. This temperature profile was obtained experimentally at Dalhousie University, Canada (see Appendix B for detailed temperature profile.)

e) At the axis:

$$V_r=V_\varphi=0\ ;\ \frac{\partial V_z}{\partial R}=0\ ;\ \frac{\partial\theta}{\partial R}=0\ ;\ \frac{\partial C}{\partial R}=0 \quad (10)$$

SOLUTION TECHNIQUE AND MESH SENSITIVITY

The finite element method is utilized and the model is divided into elements and subsequently nodes by which all the variables, which are the three velocities, concentration, pressure and the temperature can be evaluated and analyzed. In this model, which has over fourteen thousands nodes, the Galerkin finite element method approximation has been employed for silicon concentration and velocity in the solvent region along the three axes (V_r, V_φ, V_z). The governing equations are then solved simultaneously under a set of convergence criteria on the aforementioned variables. Convergence is achieved whenever:

$$\|\Delta u_i\|/\|u\|\le\varepsilon_u \qquad \Delta u_i=u_i-u_{i-1} \qquad \|R_i\|/\|R_0\|\le\varepsilon_F \quad (11)$$

where "u_i" represents the pressure, temperature, velocities and silicon concentration, along r-, φ- and z- directions for each node and "R_0" is a reference vector; typically $R(u_i)$ which is the residual force vector. ε_u is the convergence tolerance based on the relative error and ε_F is the residual convergence tolerance for each variable at each iteration [10]. Since both Δu_i and $R(u_i)$ tend to zero near the solution therefore problem is assumed converged when system satisfies the above criteria which was specified as 10^{-4} for both solution vector and residual force vector. For our study the maximum number of nonlinear iterations for both fluid and structural problem is set to 500. The norm $\|\ \|$ is a root mean square norm summed over all the equations for the model.

In order to have the best and most reliable results, an optimum number of nodes and elements should be defined, therefore, mesh sensitivity analysis was carried out and ideal numbers of nodes on both circumferential and axial edges were selected based on the average Nusselt number in solvent region. As it can be read from the Figure 2, a mesh with 40 nodes in the radial direction and 80 nodes in the axial direction leads to a value of the Nusselt number that remains (almost) the same as with finer meshes. For this and the aforementioned reasons, the 40×80 mesh combination reasonably meets the computational need and simulation becomes satisfactory for the analysis in this study.

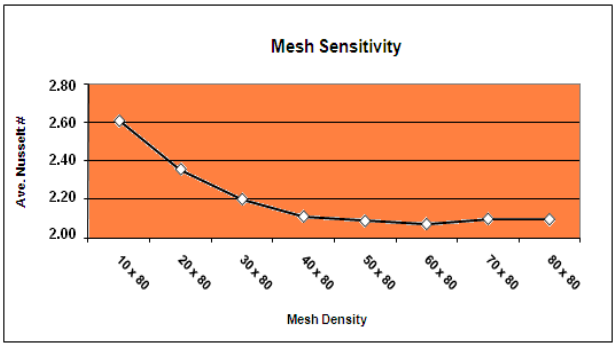

Figure 2 Mesh density vs. Nusselt number

RESULTS AND DISCUSSION

Terrestrial condition with no magnetic field. Figure 3 shows both a vertical cross section view (a: 1,2,3) of the solvent region passing through the *z*-axis of the model and a horizontal cross section (b: 1,2,3) at z = 0.1 cm above growth interface which reveals the concentration of Si in the solvent region in the terrestrial condition. It is clear that due to buoyancy induced convection there are three cells (pockets) of movement in the solvent region; which is not desirable. (a1) which is *z*-component of the velocity shows that there are three zones formed with g = 2.2 mm/s, f =1.5 mm/s and h = 0.17 mm/s respectively; this prohibits a uniform flat build-up of silicon at the interface.

Figure 3-(a3) reveals the temperature distribution along the *z*-axis and again shows the convex curvature near the interface which is not desirable.

Applied static magnetic field. The aim of any melt growth processing control is to provide conditions which give a crystal well defined compositional and structural properties. Since unsteady convection is always undesirable, the use of external body force such as magnetic field can be an alternative to suppress the unsteady convection and the effect of that can be investigated.

Figure 4 which is a line plot of silicon distribution along the *z*-axis shows how unevenly the silicon is spread out no matter how strong the applied axial magnetic force is, the result has the same distribution along the *z*-axis. Figure 5, shows the velocities along the *z*-axis passing through the origin of the vertical Bridgman model (VBM) under the influence of different intensities of applied axial static magnetic field (SMF): 2mT, 1.0 and 5.0 T (Tesla); these are compared with the case without any magnetic applied. It clearly shows that the SMF has not a very significant effect on the velocity and consequently on the flow and distribution of the silicon in the solvent region. It is obvious, however that the magnetic field acting as an external body force has no effect on the solid (seed) section of this model. Figure 5 depicts, all cases (B = 0, 2mT, 1 T and 50 T) have no major impact on the flow velocity.

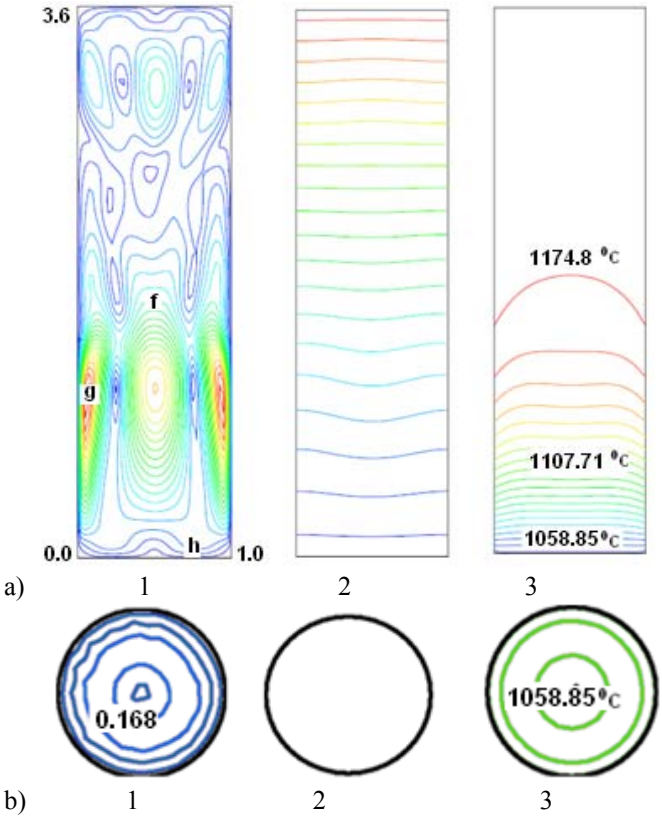

Figure 3 Vertical Bridgman, Terrestrial, with no applied magnetic field:
(1: *z*-velocity; 2: concentration; 3: temperature)
a) Model section along the *z*-axis
b) |Cross-section at z = 1 mm above growth interface

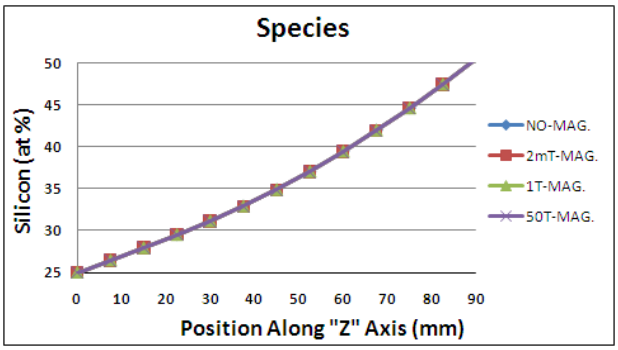

Figure 4 Silicon concentration along the *z*-Axis

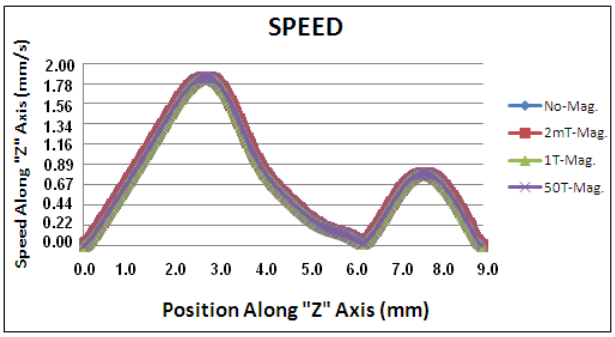

Figure 5 Velocities along the *z*-axis in VBM

CONCLUSION

A numerical modeling and simulation of single bulk crystals of $Si_{0.25}Ge_{0.75}$ growth with Si rich was conducted to investigate the effect of static magnetic field on the heat and mass transfer in the solvent region in vertical Bridgman furnaces. The curvature and shape of the silicon concentration in the process of crystallization near the growth interface were also examined. Different magnetic field intensities were applied. The meridianal as well as the azimuthal flows in the solvent region under the applied polynomial temperature along the vertical axis of the model in VBM were investigated. The static magnetic field is found to have no significant impact on the flow; thence the use of axial static magnetic field does not help to improve the process.

ACKNOWLEDGMENTS

The authors would like to thank Natural Science and Engineering Council of Canada (NSERC) for their financial support on this study.

REFERENCES

[1] IUPAC: *International Union of Pure and Applied Chemistry Report, Internet edition on Semiconductors,* Vol. 54, 1982, pp. 1533.
[2] K. Hoshikawa**,** *Japan. J. Appl. Phys*. Vol. 21, 1982, pp. 9-.
[3] S.A. Nikitin, V.I. Poleshaev and A.I. Fedyushkin., *Journal of Crystal Growth* Vol. 52, 1981, pp. 471-.
[4] C.J. Chang, R.A. Brown, *Journal of Crystal Growth*, *Vol.* 63, 1983 pp. 343-.
[5] J.A. Burton, R.C Prim and W.P. Slichter, *Journal of Chem. Phys*,. 1987, pp. 1953-.
[6] S. Meyer, A.G. Ostrogorsky, *Journal of Crystal Growth*, Vol. 171, 1997, pp. 566-576.
[7] T.W. Fu and W.R. Wilcox, *Journal of Crystal Growth*, Vol. 48, 1980, pp. 416-.
[8] T. Jasinsky and A.F. Witt, *Journal of Crystal Growth*, Vol. 67, 1984, pp. 173-.
[9] Y.C Liu, Y. Okano, S. Dost, *Journal of Crystal Growth*, Vol. 244, 2002, pp. 12-26.
[10] FIDAP 8.7 user's manual.
[11] D.T-J. Hurle, R.W. Series. "Handbook of Crystal Growth, B-Growth mechanics and dynamics," North-Holland, Amsterdam, 1994.

APPENDIX A

Figure A1 illustrates the magnetic field convention [11].

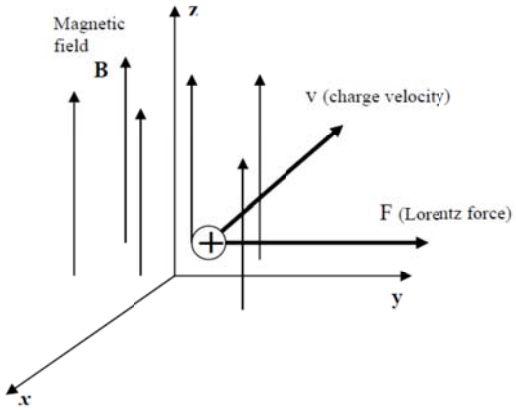

Figure A1 The magnetic force convention

APPENDIX B

The polynomial heating profile, below, is plotted based on the polynomial obtained from the Dalhousie University which an experimented result is taken from the center of the model.

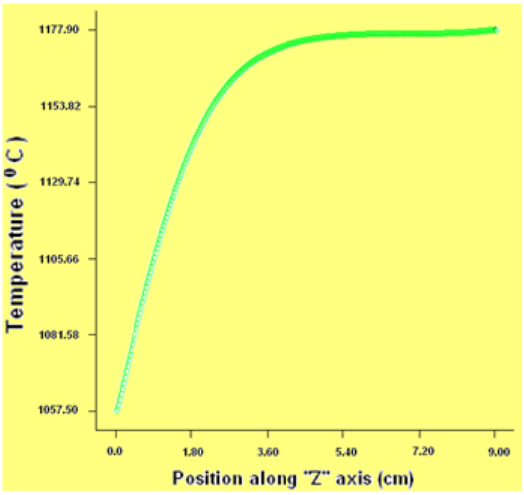

Figure B1 Temperature profile

This profile reveals that the temperature at dissolution interface, at top, is 1177.9 ºC and at the bottom, growth interface is 1057.5 ºC in solvent region only.